文章编号: 1001-9014(2019)04-0412-07
DOI:10.11972/j.issn.1001-9014.2019.04.004

Simulation and fabrication of 1.55 μm AlGaInAs/InP quantum well lasers with low beam divergence

XIONG Di[1,2], GUO Wen-Tao[1*], GUO Xiao-Feng[1], LIU Hai-Feng[1,2], LIAO Wen-Yuan[1,2], LIU Wei-Hua[1,2], ZHANG Yang-Jie[1,2], CAO Ying-Chun[1], TAN Man-Qing[1,2*]

(1. State Key Laboratory of Integrated Optoelectronics, Institute of Semiconductors, Chinese Academy of Sciences, Beijing 100083, China;
2. Center of Materials Science and Optoelectronics Engineering, University of Chinese Academy of Sciences, Beijing 100049, China)

Abstract: 1.55 μm AlGaInAs/InP quantum well lasers with low beam divergence have been theoretically designed and experimentally fabricated. An asymmetrical mode expand layer (MEL) was inserted in lower cladding to expand near field intensity distribution and decrease internal loss. Simulation results showed that the use of MEL didn't influence the laser performance negatively but dramatically decreased the vertical beam divergence at the cost of slightly increase of threshold current. And the experiment results showed high agreement to it. With a 4 μm-wide and 1 000 μm-long ridge waveguide laser with MEL, the threshold current and output power of single facet without coating is 56 mA and 17.38 mw@120 mA, and the slope efficiency is 0.272 W/A. The vertical beam divergence is 29.6° and decreases about 35.3% compared to that of typical lasers.

Key words: InP-based lasers, beam divergence, intensity distribution
PACS: 42.55.-f, 42.55.Px, 42.60.Jf, 78.55.Cr

1.55 μm AlGaInAs/InP 小发散角量子阱激光器的仿真和制备

熊 迪[1,2], 郭文涛[1*], 郭小峰[1], 刘海峰[1,2], 廖文渊[1,2],
刘维华[1,2], 张杨杰[1,2], 曹营春[1], 谭满清[1,2*]
(1. 中国科学院半导体研究所 集成光电子国家重点实验室,北京 100083;
2. 中国科学院大学 材料科学与光电工程中心,北京 100083)

摘要:理论仿真和实验制备了 AlGaInAs/InP 材料 1.55 μm 小发散角量子阱激光器. 为了扩展近场光场并减小内损耗,将一个非对称模式扩展层插入到外延结构的下盖层当中. 仿真结果表明,该模式扩展层除了少量增加激光器阈值电流以外,在不影响激光器其它性能的情况下能显著减小激光器的垂直远场发散角. 实验结果与理论仿真高度吻合. 成功制备出脊宽4 μm,腔长1000 μm 的脊波导小发散角激光器. 在端面未镀膜的情况下,该激光器阈值电流为 56 mA,输出功率为 17.38 mw@120 mA,斜率效率可以达到 0.272 W/A. 实验测得垂直远场发散角为 29.6°,相比较传统激光器减小了约 35.3%.

关 键 词:铟磷基激光器;发散角;光场分布
中图分类号:O47 **文献标识码**:A

Introduction

Due to minimal optical-fiber dispersion and loss, semiconductor diode lasers operating at 1.3 μm and 1.55 μm with low divergence are of great importance to optical interconnections and optical fiber communications. However, conventional edge-emitting quantum well lasers have small active area and tight optical confinement which have caused a large beam divergence in the direction perpendicular to the junction plane. The far field is typically about 10° ~ 30° in the horizontal direction and 40° ~ 60° in the vertical direction for InP-based lasers. And this strongly elliptical beam reduces the coupling

Received date: 2019-02-02, **revised date**: 2019-05-05 **收稿日期**:2019-02-02, **修回日期**:2019-05-05
Foundation items: Supported by the Joint Science Foundation of Chinese Academy of Science.
Biography: XIONG Di (1992-), male, Xiantao, China, Ph. D. Research area involves semiconductor lasers and photoelectric device. E-mail: xiongdi@semi.ac.cn
* **Corresponding author**: E-mail: mqtan@semi.ac.cn

efficiency and coupling tolerance between lasers and coupling optics.

Many works have been done to reduce vertical beam divergence. GaAs-based lasers emitting at a wavelength between 800 ~ 1060 nm with small beam divergence have been achieved by many ways, such as using large optical cavity (LOC) or super-large optical cavity (SLOC)[1-2], engineering the cladding layers with passive waveguides inserted[3-4] or low refractive index layers inserted[5-6], a-dopting low index quantum barriers[7-8]. Most of them make a tradeoff between optical confinement and mode size, and suffer from high threshold current, big side lobes or multimode output risks. While approaches with surface plasmonic nanostructures[9] or longitudinal photonic band crystal (PBC) designs[10-13] require thick and complex epitaxial structures, approaches monolithically integrated with spot size converters[14] require precision etch and regrowth process.

Nevertheless, there are few researches about laser emitting at 1.55 μm with small beam divergence[15-16]. The confinement factor in InP-based lasers is higher than that in GaAs-based lasers, which makes it harder to decrease vertical beam divergence.

Compared to InGaAsP/InP material ($\Delta E_c = 0.4\Delta E_g$), AlGaInAs/InP material ($\Delta E_c = 0.72\Delta E_g$) has a lager conduction band offset and reduces carrier leakage from the quantum-well region[17]. As the AlGaInAs quaternary material has higher refractive index than an InGaAsP quaternary material of the same bandgap[18], which also makes it difficult to decrease vertical beam divergence, the AlGaInAs waveguide provides not only excellent carrier confinement but also good optical confinement.

In this paper, we propose a simple effective way to reduce beam divergence by using a asymmetric mode expansion layer (MEL) without obvious performance deterioration and we present a comprehensive discussion on the design and optimization of AlGaInAs /InP $\lambda \sim 1.55$ μm lasers with small beam divergence, which shows a great agreement with experiment results. Through asymmetric mode expansion layer, more parameters can be utilized. The optical field is pulled away from p-cladding and extends into lower layers which reduces the internal loss[19] and decreases beam divergence without large side lobes or obvious confinement deterioration. In addition, it doesn't need an overgrowth process and can be fabricated as conveniently as conventional ridge lasers.

1 Epitaxial structure design and simulation

Figure 1(a) illustrates a typical refractive index profile and near-filed distribution of 1.55 μm laser with graded-index separated confinement heterostructure (GRINSCH). After detailed simulation, the strain-compensated multiple quantum wells (SC-MQW) structure has been used. The epitaxial structure contains an active region with three compressively strained (+1.2%), 6 nm thick, $Al_{0.08}Ga_{0.22}In_{0.7}As$ quantum wells (QW) and four tensile strained (-0.5%), 9 nm thick barriers, which is sandwiched by two 0.1 μm-thick GRINSCH layers. The Al composition of GRINSCH layers changes from 0.178 near active region to 0.474 near AlInAs carrier blocking layers. The carrier blocking layers utilize asymmetric structure with 140 nm thick in n-side and 50 nm thick in p-side to expand optical field into n-cladding, which reduces the internal loss since p-cladding absorption is the main contributor to it[20].

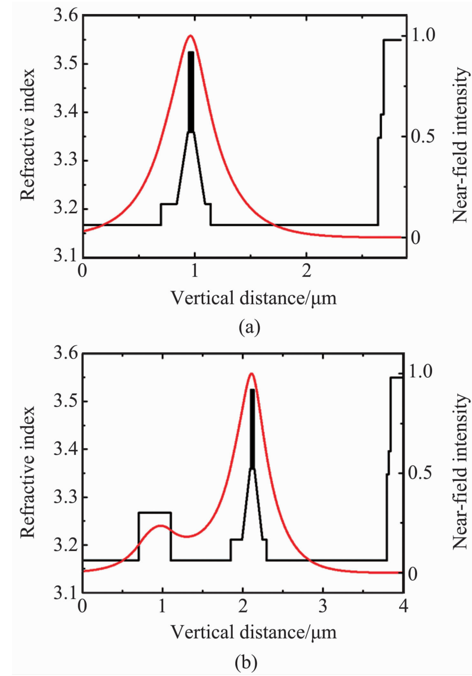

Fig. 1 Refractive index profiles (left axes) and near-filed intensity distribution (right axes) of conventional (a) and special asymmetric MEL (b) lasers

图 1 传统结构(a)和特殊非对称 MEL 结构(b)激光器折射率(左轴)和近场光场(右轴)分布示意图

We get the band parameters and refractive indices of the materials referring to Refs. [21-24]. The near optical field is calculated by solving one dimensional Helmholtz equation with MATLAB software. And the far field pattern can be obtained by taking the Fourier transformation of the near optical field. The field intensity versus angle θ is written as[25]:

$$I(\theta) \propto \frac{\cos^2\theta}{\lambda_0 r}\left|\int_{-\infty}^{\infty} E_y(x,0)\exp(ik_0 x\sin\theta)\,dx\right|^2 , \quad (1)$$

where $E_y(x,0)$ is the electric field distribution at the laser facet. The terms r, θ are the distance from the output facet and the angle relative to the waveguide axis, respectively. The term λ_0 is the emission wavelength in free space. For the fundamental mode, the beam divergence is defined as the full width at half maximum (FWHM) of the far field pattern. The far field distribution corresponding to widen near optical field exhibits smaller beam divergence.

The threshold current density J_{th} for conventional quantum-well lasers can be well approximated as the exponential expression[26]:

$$J_{th} = \frac{J_0}{\eta_i}\exp\left(\frac{\alpha_t}{\Gamma\beta_0 J_0}\right) , \quad (2)$$

where J_0 is the transparent current density, η_i is the internal quantum efficiency, α_t is the total loss including the internal material loss and mirror loss, Γ is the optical confinement factor, and β_0 is the gain coefficient.

From the Eqs. (1-2), we can see a tight trade-off between the optical confinement factor (threshold current density) and the beam divergence. The calculated optical confinement factor of the typical laser is 2.93% with 45.72° vertical beam divergence. And this tightness can be solved by the insertion of a mode expansion layer in the n-cladding layer, which provides an additional degree of freedom in the device design. The MEL is a passive waveguide that has a refractive index lower than that of the core waveguide but higher than that of the claddings, and it can expand the optical field slightly into lower cladding and suppress higher mode lasing. For the fundamental mode, the optical confinement Γ' of laser with MEL can be written as[27]:

$$\Gamma' = \left[1 + \frac{2}{(c+d)^2}\right]^{-1}\Gamma \quad , \quad (3)$$

where

$$c = \frac{n_{\mathrm{eff2}} - n_{\mathrm{eff1}}}{2\kappa} \quad , \quad (4)$$

$$d = \sqrt{c^2 + 2} \quad , \quad (5)$$

where n_{eff1} and n_{eff2} are the effective refractive indices for the passive waveguide and uncoupled core waveguide, respectively. κ is the coupling coefficient between core waveguide and the passive waveguide. Since all the parameters except Γ and α_t of expression (2) are independent (J_0 and β_0 dependent only on the active region) of whether the MEL is inserted, and the existence of passive waveguide causes only a very small amount of increase in material loss which can be ignored, the threshold current density for lasers with mode expansion layer can be written as[27]:

$$J_{\mathrm{th}}' = \frac{J_0}{\eta_i}\exp\left(\frac{\alpha}{\Gamma' b_0 J_0}\right) = J_{\mathrm{th}}\exp\left[\frac{2}{(c+d)^2}\frac{\alpha_t}{\Gamma b_0 J_0}\right] \quad . \quad (6)$$

Clearly, the threshold current density for the mode expansion structure is always larger than that for the conventional structure, because the exponent is always positive. But the threshold current density J_{th}' can remain insensitive to MEL by designing suitable c to make the argument of the exponential function small[27]. Since n_{eff2} is greater than n_{eff1} to guarantee a fundamental mode emission, the value of κ and n_{eff1} should be small to obtain a suitable c and further to get a small argument of the exponential function. The parameters used for optimization are: the separation distance (D) between the GRINSCH and MEL, the thickness (T) of the MEL, and the composition (Q) of the MEL, as showed in Fig. 1(b). To avoid a large index of MEL and big band offset in n-cladding, we choose 1.06Q (InP lattice-matched InGaAsP with a bandgap wavelength of 1.06 μm) and 1.1Q to be the composition of the MEL.

Figure 2 shows the calculated optical confinement factor Γ' and vertical FWHM θ as functions of the separation distance D (a) and the thickness T of the MEL (b) when the composition is 1.06Q. As showed in Fig. 2(a), when T is fixed at 200 nm, with the increase

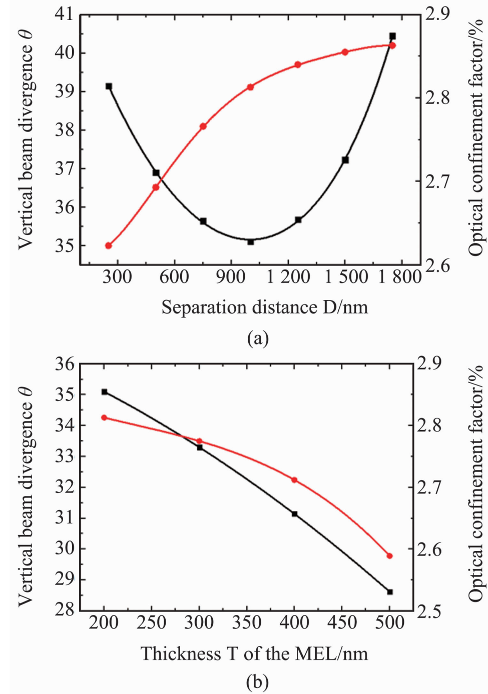

Fig. 2 Calculated optical confinement factor Γ' and vertical FWHM θ versus the separation distance D (a) and the thickness T of the MEL (b) when the composition is 1.06Q. T is fixed at 200 nm in (a) and D is fixed at 1 000 nm in (b)

图 2 在组份为 1.06 Q 时,模拟的限制因子和垂直远场发散角随分隔距离 D(a)和 MEL 的厚度 T(b)之间的关系.(a)中 T 为 200 nm,(b)中 D 为 1 000 nm

of D, the vertical beam divergence decreases from 39.15° to 35.1° and then increases to 40.45° while the confinement factor has a little increase, but is still lower than that of conventional laser without MEL. This is due to the inserted MEL which expands the near filed distribution and a larger D will decrease the vertical beam divergence but a too large D will weak the influence of EBL to active region and can't expand near optical filed efficiently. As D increasing, the coupling coefficient κ between core waveguide and MEL decreases, leading to larger c and Γ'. When D is fixed at 1 000 nm showed in Fig. 2(b), the increasing T causes lower Γ' and smaller vertical beam divergence. As T increases, the refractive index of EBL increases, and more light has been expanded into lower cladding result in lower and smaller vertical divergence. But from Fig. 3 we can see the effect of EBL to active region is still small even when the T is increased to 500 nm. This is because the refractive index of 1.06Q EBL ($n_{1.06\,\mathrm{Q}} = 3.25$) is too small compared to that of the active region ($n_{\mathrm{ac}} = 3.5$) and the EBL can only confine a small amount of optical field. And then we fixed the composition to be 1.1Q ($n_{1.1\,\mathrm{Q}} = 3.28$), D to be 750 nm and 1 000 nm.

Figure 4 shows the calculated optical confinement factor Γ' and vertical FWHM θ versus the thickness T of the MEL when the composition is 1.1Q under different D. Figure 5 shows some of the near field intensity distri-

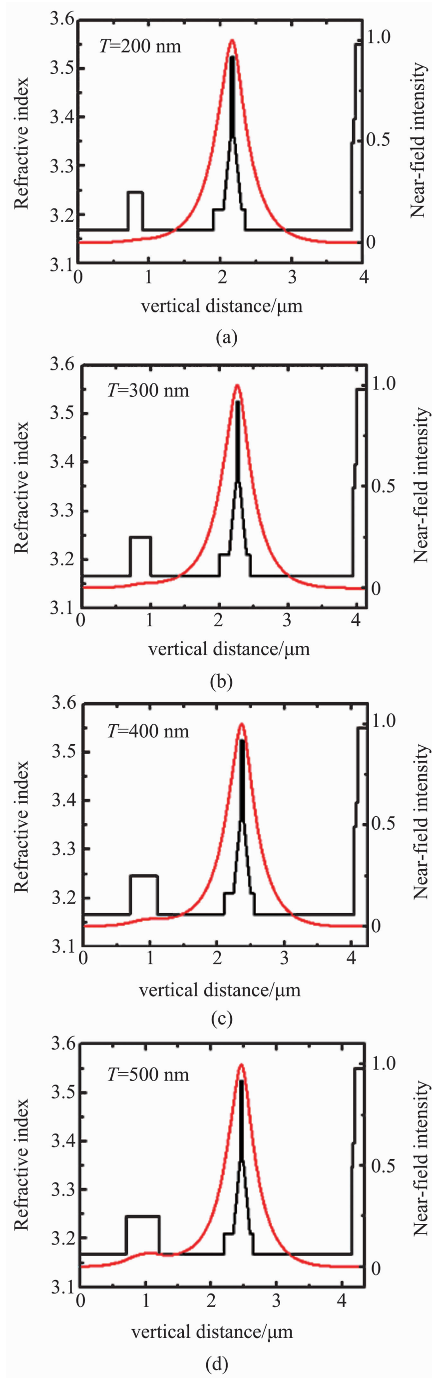

Fig. 3　Near field intensity distributions under different T with D = 1 000 nm and 1.06 Q
图 3　组份为 1.06 Q 和 D = 1 000 nm 时，在不同 T 值下近场光场的分布

butions. It has a much better effect of MEL to active region and shows the similar tendency when the composition of MEL is 1.1 Q compared to 1.06 Q. And the structure with 1 000 nm MEL has a smaller vertical beam divergence and a larger optical confinement factor under the same thickness of MEL in comparison with the structure with 750 nm MEL. Side lobes may appear when the thickness of MEL is large to 500 nm, as showed in Fig.

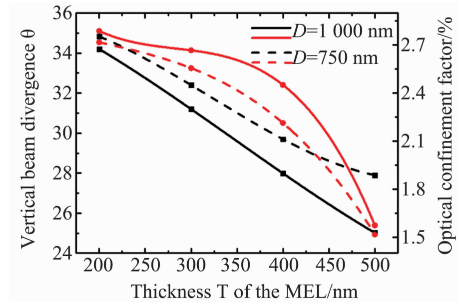

Fig. 4　Calculated optical confinement factor and vertical FWHM versus the thickness T of the MEL when the composition is 1.1Q. Solid line is D = 1 000 nm and dashed line is D = 750 nm
图 4　当组份为 1.1Q 时，模拟的限制因子和垂直远场发散角随 MEL 的厚度 T 之间的关系. 实线为 D = 1 000 nm，虚线为 D = 750 nm

5 (b) and (d). And side lobes can lower the coupling efficiency and coupling tolerance between lasers and coupling optics which should be avoid. Moreover, when T is 500 nm, no matter the D is 750 nm or 1 000 nm, the optical confinement factors suffer a significant decrease and it will lead to a large threshold current density.

Finally, we choose the value of the separation distance (D) between the GRINSCH and MEL as 1 000 nm, the thickness (T) of the MEL as 400 nm, and the composition (Q) of the MEL as 1.1Q. The calculated optical confinement factor of this special laser with EBL is 2.45% with 27.99° vertical beam divergence. The optical confinement factor only decrease by 0.45% (16.3%) while the vertical beam divergence reduces by 17.73° (38.8%) compared with that of the typical structure. We investigated the light - current - voltage (L-I-V) characteristics of both typical and special structures by using commercial available LASTIP (LASer Technology Integrated Program) simulation software, as showed in Fig. 6. The threshold current of the special structure with MEL is slightly higher than that of typical structure because of a smaller optical confinement factor. But the slope efficiencies as well as the series resistance of both structures are almost equal, indicating that the inserted MEL barely has negative effect on laser performance.

The variation of threshold current with temperature can be written as:

$$I_{\mathrm{th}}(T) = I_{\mathrm{th}}(T_r)\exp\left(\frac{T - T_r}{T_0}\right) \quad , \quad (7)$$

where $I_{\mathrm{th}}(T)$ and $I_{\mathrm{th}}(T_r)$ are threshold currents at temperature T and room temperature T_r, respectively. T_0 is the characteristic temperature. The characteristic temperature can be calculated by linear fitting between temperature and threshold current, as showed in Fig. 7. The characteristic temperature of typical structure and special structure with MEL are 105.8 K and 102.1 K respectively between 296 K and 326 K, which are both much higher than that (65 K) of InGaAsP/InP material. It indicates that the inserted MEL will not affect the temperature characteristic of laser negatively.

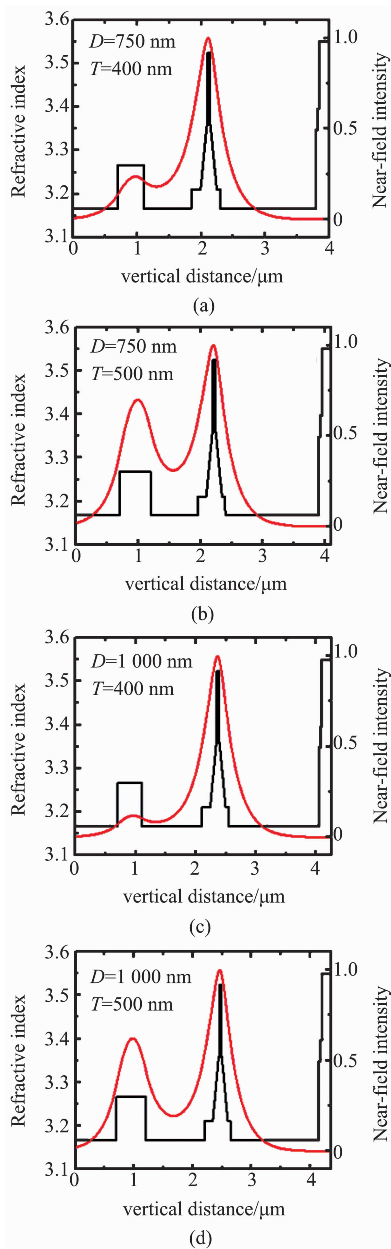

Fig. 5 Near field intensity distributions under different D and T with 1.1Q MEL

图 5 当 MEL 组份为 1.1Q 时,在不同 D 值和 T 值下近场光场的分布

2 Device fabrication and test results

Table 1 shows the details of the epitaxial structure of the special designed laser with mode expand layer. It's similar to typical laser described previous except a 1.1Q MEL with the thickness of 400 nm is inserted at lower cladding 1 000 nm away from active region, and it doesn't require a regrowth process. After growth, the sample was patterned into ridge waveguide lasers. The total FP cavity length is 1 000 nm and the ridge waveguide is 4 μm wide and 1.6 μm high. A 2 μm wide window in the ridge is used for current injection. The dry etching process was designed to stop 100 nm above the active region, but in fact it might etched over a little depth which could lead to an increase of threshold current.

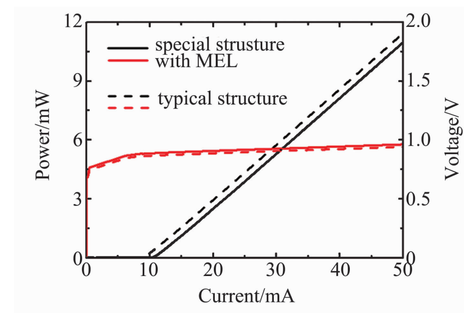

Fig. 6 The simulated L-I-V characteristics of typical structure (dashed-line) and special structure with MEL (solid-line)

图 6 模拟的传统结构(虚线)和特殊 MEL 结构(实线)激光器的 L-I-V 特性

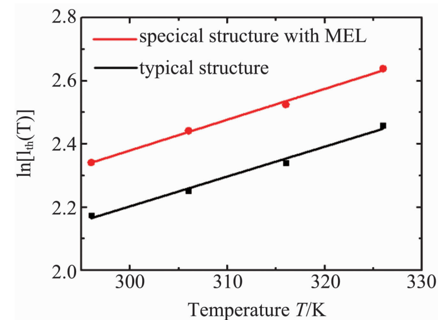

Fig. 7 The simulated relationship between threshold current and temperature of typical structure (black line) and special structure with MEL (red line)

图 7 模拟的传统结构(黑线)和特殊 MEL 结构(红线)激光器的阈值电流和温度之间的关系

At last, the sample was cleaved into individual laser bars with both facets left uncoated. The devices were mounted p-side up on an AlN heat sink with temperature controlled at 296 K and tested under CW conditions.

Table 1 Layer Structure of the 1.55 μm laser with mode expansion layer

表 1 拥有模式扩展层的 1.55 μm 激光器外延层结构

Material	Thickness/nm	Doping Type	Concentration /cm^{-3}	Notes
$In_{0.53}Ga_{0.47}As$	150	P	$>1\times10^{19}$	
$In_{0.63}Ga_{0.37}As_{0.8}P_{0.2}$	25	P	$>1\times10^{18}$	1.5Q
$In_{0.71}Ga_{0.29}As_{0.62}P_{0.38}$	25	P	$>1\times10^{18}$	1.3Q
InP	1 100	P	5×10^{17}	
InP	400	P	3×10^{17}	
$In_{0.526}Al_{0.474}As$	50	Undoped		
$Al_xGa_{0.474-x}In_{0.526}As$	100	Undoped		
3×QWs $Al_{0.08}Ga_{0.22}In_{0.7}As$	6×3	Undoped		1.2% C
4×Barriers AlGaInAs	9×4	Undoped		-0.5% T
$Al_xGa_{0.474-x}In_{0.526}As$	100	Undoped		
$In_{0.526}Al_{0.474}As$	140	N	8×10^{16}	
InP	1 000	N	1×10^{17}	
$In_{0.85}Ga_{0.15}As_{0.33}P_{0.67}$	400	N	3×10^{17}	1.1Q
InP	700	N	3×10^{17}	
InP Substrate S-Doped 2 ~ 8 $\times10^{18}$ 350 μm				

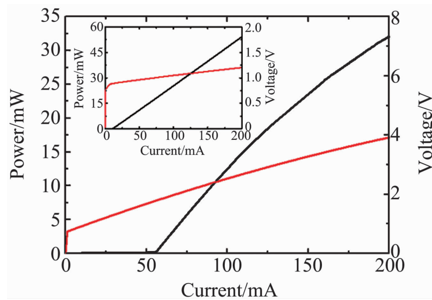

Fig. 8 Measured and simulated (inset) *L-I-V* characteristics of special designed laser with MEL at 296 K
图 8 在 296 K 温度下,特殊 MEL 结构激光器的 *L-I-V* 特性测试和模拟(小图)

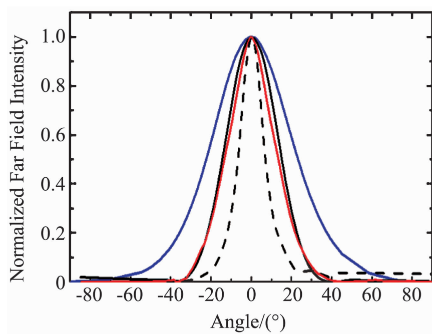

Fig. 9 Far field intensity distributions of typical laser (blue-line, $\theta_{\perp}$ = 45.72 °), simulated special laser (red-line, $\theta_{\perp}$ = 27.99°) and tested special laser (black-solid-line, $\theta_{\perp}$ = 29.6°, black-dashed-line, $\theta_{//}$ = 15.5°) with MEL at 160 mA
图 1 在 160 mA 注入电流下,传统结构激光器(蓝线,$\theta_{\perp}$ = 45.72°),模拟的特殊 MEL 结构激光器(红线,$\theta_{\perp}$ = 27.99°)和测试的特殊 MEL 结构激光器(黑实线,$\theta_{\perp}$ = 29.6°,黑虚线,$\theta_{//}$ = 15.5 °)的远场强度分布

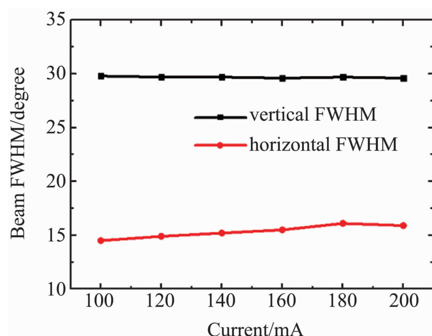

Fig. 10 Measured far field beam divergence under different injection currents
图 10 测试的远场垂直发散角随注入电流的变化

Figure 8 shows the measured and simulated *L-I-V* characteristics of special designed laser with MEL at room temperature. The measured threshold current is 56 mA, a little higher than the value of simulation because of processing step. Over-etching might lead to higher internal loss as well as the threshold current because of the increase of non-radiative recombination near the active region. Annealing for ohmic metallization with a comparatively high temperature made ohmic contact imperfect and caused a higher series resistance (15 Ω) than usual (4 Ω). The simulated value of series resistance (2.25 Ω) is close to normal condition. However, the output power achieves 17.38 mW@120 mA and the slope efficiency is 0.272 W/A, similar to the value 0.278 W/A of simulation and much higher than that reported in Ref. [15]. The divergence angles for the horizontal and vertical direction are 15.5° and 29.6°, respectively. And the vertical divergence shows highly consistent with the simulation value 27.99°, also as the far field intensity distribution. It has decreased about 35.3% compared to that of typical laser as showed in Fig. 9, which indicates that the inserted MEL can expand near field distribution and lower vertical beam divergence effectively.

Figure 10 shows the stability of the far field beam divergence at different injection currents. The laser works under fundamental mode at all level injection currents. The vertical FWHM barely varies with the injection current while the horizontal FWHM increases slightly with the increase of the injection current, which result from the ridge waveguide index changes caused by thermal and carrier injection effects. The aspect ratio ranges from 2.06 to 1.84 vary with the change of injection current and consistently demonstrates better performance as the typical aspect ratio of conventional lasers is about 3.

3 Conclusions

In summary, a special designed 1.55 μm laser based on AlGaInAs/InP material with small beam divergence has been reported by simulation and experiment. An asymmetrical mode expand layer (MEL) has been inserted in lower cladding to expand near field intensity distribution and decrease vertical beam divergence. As showed by simulation, the inserted MEL barely have negative influence on laser performance, and the whole structure doesn't need a regrowth process. For 4 μm-wide and 1 000 μm-long ridge waveguide lasers, the threshold current is 56 mA, and the output power is 17.38 mw@120 mA. The slope efficiency of 0.272 W/A has been achieved. The horizontal and vertical beam divergence of the laser is 15.5° and 29.6°, respectively, which shows a high agreement with the simulation results. The vertical beam divergence has decreased about 35.3% compared to that of typical lasers. And the far field intensity distribution also shows a high stability for injection current.

References

[1] Gordeev N Y, Payusov A S, Shernyakov Y M, *et al*. Transverse single-mode edge-emitting lasers based on coupled waveguides[J]. *Optics Letters*, 2015, **40**(9):2150-2.

[2] Pietrzak A, Wenzel H, Crump P, *et al*. 1060-nm ridge waveguide lasers based on extremely wide waveguides for 1.3 W continuous-wave emission into a single mode with FWHM divergence angle of $9^{\circ}\times 6^{\circ}$ [J]. *IEEE Journal of Quantum Electronics*, 2012, **48**(5):568-575.

[3] Qiu B, Mcdougall S D, Liu X, *et al*. Design and fabrication of low beam divergence and high kink-free power lasers[J]. *IEEE Journal of*

Quantum Electronics, 2005, **41**(9):1124-1130.

[4] Wenzel H, Bugge F, Erbert G, *et al*. High-power diode lasers with small vertical beam divergence emitting at 808 nm[J]. *Electronics Letters*, 2001, **37**(16):1024.

[5] Hung C T, Lu T C. 830-nm AlGaAs-InGaAs graded index double barrier separate confinement heterostructures laser diodes with improved temperature and divergence characteristics[J]. *IEEE Journal of Quantum Electronics*, 2013, **49**(1):127-132.

[6] Yang G, Smith G M, Davis M K, *et al*. High-performance 980 nm ridge waveguide lasers with a nearly circular beam[J]. *IEEE Photonics Technology Letters*, 2004, **16**(4):981-983.

[7] Crump P, Pietrzak A, Bugge F, *et al*. 975 nm high power diode lasers with high efficiency and narrow vertical far field enabled by low index quantum barriers[J]. *Applied Physics Letters*, 2010, **96**(13): 131110.

[8] Pietrzak A, Crump P, Wenzel H, *et al*. Combination of low-index quantum barrier and super large optical cavity designs for ultranarrow vertical far-fields from high-power broad-area lasers[J]. *IEEE Journal of Selected Topics in Quantum Electronics*, 2011, **17**(6): 1715-1722.

[9] Yu N, Fan J, Wang Q J, *et al*. Small-divergence semiconductor lasers by plasmonic collimation[J]. *Nature Photonics*, 2008, **2**(9):564-570.

[10] Wang L, Tong C, Tian S, *et al*. High-power ultralow divergence edge-emitting diode laser with circular beam[J]. *IEEE Journal of Selected Topics in Quantum Electronics*, 2015, **21**(6): 343-351.

[11] Miah M J, Kalosha V P, Bimberg D, *et al*. Astigmatism-free high-brightness 1 060 nm edge-emitting lasers with narrow circular beam profile[J]. *Optics Express*, 2016, **24**(26):30514-30522.

[12] Liu L, Qu H, Liu Y, *et al*. Design and analysis of laser diodes based on the longitudinal photonic band crystal concept for high power and narrow vertical divergence[J]. *IEEE Journal of Selected Topics in Quantum Electronics*, 2015, **21**(1): 440-446.

[13] Zhao S, Qi A, Qu H, *et al*. Effect of ridge structure on electro-optical characteristics of ridge-waveguide lasers with low vertical divergence based on photonic crystal structure[C]//*AOPC* 2017: *Laser Components, Systems, and Applications. International Society for Optics and Photonics*, 2017, 10457: 104572B.

[14] Jeon H, Verdiell J M, Ziari M, *et al*. High-power low-divergence semiconductor lasers for GaAs-based 980-nm and InP-based 1 550-nm applications[J]. *IEEE Journal of Selected Topics in Quantum Electronics*, 1998, **3**(6): 1344-1350.

[15] Hou L P, Haji M, Akbar J, *et al*. 160-GHz 1.55-μm colliding-pulse mode-locked algainas/inp laser with high power and low divergence angle[J]. *IEEE Photon. Technol. Lett.*, 2012, **24**(12): 1057-1059.

[16] Hou L, Haji M, Akbar J, *et al*. Low divergence angle and low jitter 40 GHz AlGaInAs/InP 1.55 μm mode-locked lasers[J]. *Optics Letters*, 2011, **36**(6): 966-968.

[17] Liou B T, Yen S H, Yao M W, *et al*. Numerical study for 1.55-μm AlGaInAs/InP semiconductor lasers [C]//*Optoelectronic Devices: Physics, Fabrication, and Application III. International Society for Optics and Photonics*, 2006, **6368**: 636814.

[18] Hou L, Stolarz P, Javaloyes J, *et al*. Subpicosecond pulse generation at quasi-40-GHz using a passively mode-locked AlGaInAs-InP 1.55- $ \mu {\hbox {m}} $ strained quantum-well laser[J]. *IEEE Photonics Technology Letters*, 2009, **21**(23): 1731-1733.

[19] Garbuzov D, Xu L, Forrest S R, *et al*. 1.5/spl mu/m wavelength, SCH-MQW InGaAsP/InP broadened-waveguide laser diodes with low internal loss and high output power[J]. *Electronics Letters*, 1996, **32**(18): 1717.

[20] Joindot I, Beylat J L. Intervalence band absorption coefficient measurements in bulk layer, strained and unstrained multiquantum well 1.55 mu m semiconductor lasers[J]. *Electronics Letters*, 1993, **29**(7): 604-606.

[21] Minch J, Park S H, Keating T, *et al*. Theory and experiment of In Ga As P and In Ga Al As long-wavelength strained quantum-well lasers [J]. *IEEE J. Quantum Electron*, 1999, **35**(5): 771-782.

[22] Vurgaftman I, Meyer J R, Ram-Mohan L R. Band parameters for III-V compound semiconductors and their alloys[J]. *Journal of Applied Physics*, 2001, **89**(11): 5815-5875.

[23] Selmic S R, Chou T M, Sih J P, *et al*. Design and characterization of 1.3-/spl mu/m AlGaInAs-InP multiple-quantum-well lasers [J]. *IEEE Journal of selected topics in Quantum Electronics*, 2001, **7**(2): 340-349.

[24] Ivanov A V, Kurnosov V D, Kurnosov K V, *et al*. Refractive indices of solid AlGaInAs solutions[J]. *Quantum Electronics*, 2007, **37**(6): 545.

[25] Liu D C, Lee C P, Tsai C M, *et al*. Role of cladding layer thicknesses on strained - layer InGaAs/GaAs single and multiple quantum well lasers[J]. *Journal of Applied Physics*, 1993, **73**(12): 8027-8034.

[26] Yang G W, Xu J Y, Xu Z T, *et al*. Theoretical investigation on quantum well lasers with extremely low vertical beam divergence and low threshold current[J]. *Journal of applied physics*, 1998, **83**(1): 8-14.

[27] Yen S T, Lee C P. Theoretical investigation on semiconductor lasers with passive waveguides[J]. *IEEE journal of quantum electronics*, 1996, **32**(1): 4-13.